Formulation of gelled non-toxic bicontinuous microemulsions stabilized by highly efficient alkanoyl methylglucamides

*Ke Peng, Natalie Preisig, Thomas Sottmann, Cosima Stubenrauch**

Institute of Physical Chemistry, University of Stuttgart, Pfaffenwaldring 55,

70569 Stuttgart, Germany

Abstract

Gelled non-toxic bicontinuous microemulsions have a great potential for transdermal drug delivery as the microemulsion facilitates the solubilization of both hydrophilic and hydrophobic drugs, while the gel network provides mechanical stability and thus an easy application on the skin. In our previous study, we formulated a gelled non-toxic bicontinuous microemulsion: we gelled the system H_2O – IPM – Plantacare 1200 UP ($C_{12}G_{1.4}$) – 1,2-octanediol with the low molecular weight organogelator 1,3:2,4-dibenzylidene-D-sorbitol (DBS). However, a large amount of Plantacare 1200 UP (12 wt.%) is needed to form a bicontinuous microemulsion. To solve this problem, we studied a new class of surfactants, namely alkanoyl methylglucamides (MEGA), which has been rarely used for the formulation of microemulsions. The phase behavior of MEGA-8/10, MEGA-12/14-PC and MEGA-12/14-HC was compared with that of alkyl polyglucosides. We found that even with 2 wt.% MEGA-

12/14-HC a bicontinuous microemulsion can be formed, which is 1/6 of the amount of Plantacare 1200 UP. The bicontinuous microstructure of the non-toxic microemulsion H_2O – IPM – MEGA-12/14-HC – 1,2-octanediol was confirmed by small-angle neutron scattering (SANS). Furthermore, the phase boundaries remained unchanged when gelled by DBS. The rheological properties of the gel were studied by oscillatory shear rheometry. Finally, FFEM images show the coexistence of gel fibers and bicontinuous oil and water domains. These results suggest that the new gelled non-toxic bicontinuous microemulsion is an orthogonal self-assembled system.

Keywords: bicontinuous microemulsion, low molecular weight gelator, orthogonal self-assembly, alkanoyl methylglucamides

Introduction

Gelled bicontinuous microemulsions count among gelled complex fluids [1]. If the two self-assembled structures, namely the gel fibrillar network and the bicontinuous microemulsion, form independently but simultaneously, this phenomenon is called orthogonal self-assembly [2]. The gelled bicontinuous microemulsion H_2O – *n*-decane – tetraethylene glycol monodecyl ether ($C_{10}E_4$) – 12-hydroxyoctadecanoic acid (12-HOA) was proven to be orthogonally self-assembled by means of freeze-fracture transmission electron microscopy (FFEM) and small-angle neutron scattering (SANS) [3,4]. It was found that the gel fibers penetrate both the water and the oil domains, even though the low molecular weight organogelator 12-HOA only dissolves in the oil phase. In contrast to polymeric gels, molecular gels form gel fibrillar networks via the self-assembly of single molecular gelators, which are also referred to as low molecular weight gelators [5]. Due to the non-covalent interactions among gelator molecules, the gelation process is reversible. Thus the sol–gel transition can be manipulated externally, for example, by a temperature change. The thermodynamically stable bicontinuous microemulsions contain two interweaving water and oil sub-domains separated by an amphiphilic surfactant monolayer with domain sizes ranging from 5 to 100 nm [6]. Bicontinuous microemulsions provide long-term stability as well as substantially high solubilization capacity for both hydrophobic and hydrophilic components and enhance the permeation through skin barriers [7]. Therefore, gelled bicontinuous microemulsions are of particular interest in the field of transdermal drug delivery as they combine the mechanical stability of the gel network and the above-mentioned features of the bicontinuous microstructure [1].

In order to achieve transdermal drug delivery, biodegradable non-toxic microemulsions, which are suitable for biological organisms, must be formulated. Although non-toxic microemulsions as drug delivery systems have been extensively studied in pharmaceutical science [7–11], those were mostly oil-in-water (O/W) microemulsions. However, bicontinuous

microemulsions, which exhibit the most efficient solubilization and excellent wetting properties, have not been studied in detail to date. Kahlweit et al. made a series of attempts to formulate non-toxic bicontinuous microemulsions. They started with the quaternary system H_2O – *n*-alkane – lecithin – alkanol [12], then replaced the zwitterionic surfactant lecithin with non-ionic alkyl polyglucosides (or glycosides) [13]. Since *n*-alkanes are not biocompatible, they replaced *n*-alkanes with unsaturated fatty acid ethyl esters [14]. Subsequently, alkanol was replaced by 1,2-diol, which is biocompatible yet surface-active enough to act as co-surfactant [15]. Finally, due to its sensitivity to light and oxygen, the unsaturated fatty acid ethyl esters were replaced by the saturated fatty acid ester isopropyl myristate (IPM). In this way, the non-toxic microemulsion H_2O – IPM – glycoside – alkanediol was successfully formulated [16].

Following in the footsteps of Kahlweit et al., we also pursued the idea of formulating non-toxic microemulsions but extended it to a combination of non-toxic microemulsions and viscoelastic gel networks [17]. We formulated a non-toxic bicontinuous microemulsion with a technical-grade glycoside surfactant (sugar surfactant, see Figure 1, middle) and gelled the microemulsion with the low molecular weight organogelator 1,3:2,4-dibenzylidene-D-sorbitol (DBS, see Figure 1, right) [18], which did not change the phase boundaries of the microemulsion. We started the formulation of the non-toxic microemulsion with the scouting system H_2O – *n*-octane – β-C_8G_1 – 1-octanol [19,20], and replaced the oil *n*-octane and the co-surfactant 1-octanol with non-toxic isopropyl myristate (IPM) and 1,2-octanediol, respectively. However, the replacement of the oil and the co-surfactant led to a large decrease of the efficiency of the system. Generally, there are two methods for improving the efficiency. The first method is to add efficiency boosters, e.g. amphiphilic block copolymers [21,22], which, however, are not biocompatible. The other method is to find a more efficient surfactant. Besides glycosides, *n*-alkanoyl-*N*-methylglucamines (Figure 1, left), which are also called glucamides, fall into the category of sugar surfactants, too. The open-ring glucose unit is connected to the alkyl chain

by an amide bond. The methyl group at the nitrogen contributes to the water solubility of the surfactant [23]. Glucamides and glycosides have comparable properties: they are both made from renewable sources, they are biodegradable and they are dermatologically safe [24]. However, only limited studies about the phase behavior of glucamide-containing microemulsions can be found [25–27].

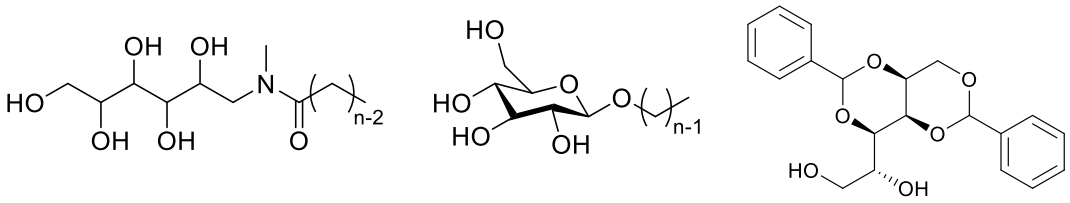

Figure 1. Molecular structures of (left) alkanoyl methylglucamide (MEGA-*n*), or *n*-alkanoyl-*N*-methylglucamine, (middle) *n*-alkyl-β-D-glucopyranoside (β-C_nG_1), (right) the low molecular weight organogelator 1,3:2,4-dibenzylidene-D-sorbitol (DBS).

With a view to filling this gap as well as to finding a highly efficient surfactant for our gelled non-toxic bicontinuous microemulsions, we studied the solubilization capacity of technical-grade glucamide surfactants with $C_{8/10}$- and $C_{12/14}$-chain lengths ($C_{8/10}$ = mixture of octyl and decyl chains; $C_{12/14}$ = mixture of dodecyl and tetradecyl chains). We formulated quaternary systems consisting of H_2O – IPM – glucamide – 1,2-octanediol and compared them with the glycoside-containing ones. One $C_{12/14}$-glucamide was found to be enormously efficient for the formation of bicontinuous microemulsions. We thus investigated this system via phase studies and small-angle neutron scattering (SANS). Finally, we gelled the non-toxic bicontinuous microemulsion with the low molecular weight organogelator DBS, which was also used to gel the non-toxic glycoside-containing microemulsions in our previous study. The gelled bicontinuous

microemulsion was subsequently characterized by rheological measurements and freeze-fracture electron microscopy (FFEM).

Experimental Section

Materials

Bi-distilled water was used to prepare all protonated samples. For SANS measurements, deuterated samples were prepared replacing bi-distilled water with deuterium oxide (> 99.9%) from Eurisotop, France. The chemicals *n*-octane (Alfa Aesar, > 98%), 1-octanol (Aldrich, 99%), isopropyl myristate (TCI, > 98%), and 1,2-octanediol (Acros, > 98%) were used as purchased. The low molecular weight organogelator 1,3:2,4-dibenzylidene-D-sorbitol (DBS) was purchased from NJC Europe under the product name "Geniset® D", and the low molecular weight hydrogelator *N*,*N*'-dibenzoyl-L-cystine (DBC, > 98%) was purchased from Santa Cruz, the USA. The technical-grade alkanoyl methylglucamides were provided by Clariant GmbH, Germany. Due to the solubility problem of glucamides in pure water, the original products contain co-solvents, and we used the surfactants as received without further purification. Three commercially available glucamides were studied during the experiments. They are named according to the main active components: (1) MEGA-8/10 (50% $C_{8/10}$-methylglucamide, 45% water, 5% propylene glycol), (2) MEGA-12/14-HC (63% $C_{12/14}$-methylglucamide, 22% water, 10% ethanol, 4.5% propylene glycol), (3) MEGA-12/14-PC (35% $C_{12/14}$-methylglucamide, 60% water, 4% propylene glycol, 0.8% sorbic acid). The CMC value of (1) is about 0.26 $g \cdot L^{-1}$ and the CMC of (2) is about 0.026 $g \cdot L^{-1}$ (see Figure S1 in SI). The CMC of (3) could not be measured due to the low solubility of the surfactant.

Sample preparation

Non-gelled microemulsions were prepared by weighing in surfactant (C), co-surfactant (D), oil (B), and water (A) with an analytical balance into glass tubes, which were then sealed by polyethylene stoppers. For monitoring phase diagrams, we used a titration procedure (explained in Section *Phase Behavior*) to reduce the amount of material. Subsequently, the samples were heated up to 50 °C in a water bath while being stirred to homogenize.

In the case of gelled microemulsions, a gelator was additionally added to the samples. The samples were firstly heated above 95 °C to dissolve the gelator. A heat gun was utilized when necessary. With DBS the gelation process takes less than 30 seconds, so the samples were quickly transferred to an ice bath directly from the 95 °C water bath with manual shaking to ensure homogeneous gelation. Afterward, the samples were transferred to a 25 °C water bath and allowed to equilibrate. It is essential to agitate the gelled microemulsion samples vigorously before gelling; otherwise, phase separation occurs, and the gelation process must be repeated.

Phase behavior

The phase behavior was investigated at a constant temperature of T = 25.0 °C in the water bath, which has a precision of ±0.1 K. The non-gelled microemulsion samples were firstly prepared without co-surfactant (D). After equilibration in the water bath, a co-surfactant (D) was added to the sample dropwise by a syringe. The added amount of co-surfactant was recorded by weight with an accuracy of ±0.001 g. After adding the co-surfactant, the sample was shaken and stirred vigorously before it was left to reach equilibrium. Then the phase behavior was visually determined. Birefringence of lyotropic liquid crystalline phases was observed via crossed polarizers. Since the phase transitions of sugar surfactant-based microemulsions were induced by a fourth component, namely a co-surfactant, the phase

behavior is presented in a phase tetrahedron (Figure 2). The phase behavior of these microemulsions is studied at a constant oil-to-water ratio, i.e. recording a two-dimensional section through the tetrahedron as highlighted in Figure 2. Hereby "$\underline{2}$" means the coexistence of an oil-in-water (o/w)-microemulsion (lower phase) and an oil excess phase (upper phase). "1" denotes the isotropic one-phase microemulsion. "$\overline{2}$" means the coexistence of an excess water phase (lower phase) and a water-in-oil (w/o)-microemulsion (upper phase). "3" denotes the coexistence of three phases, namely, an excess water phase (lower phase), a microemulsion (middle phase), and an excess oil phase (upper phase).

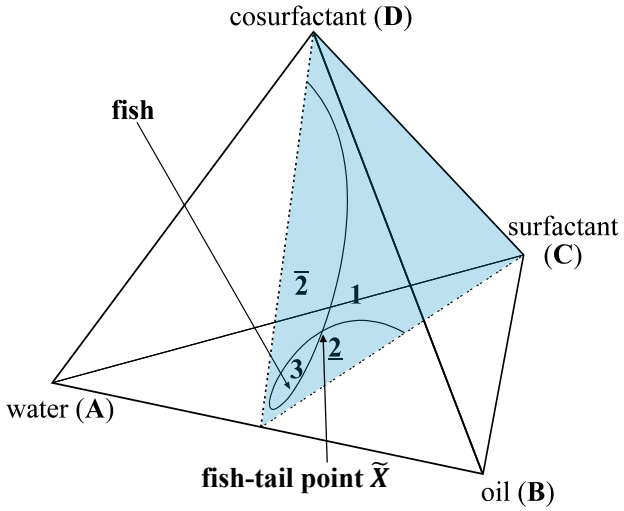

Figure 2. Schematic phase tetrahedron of a quaternary system water – oil – surfactant – co-surfactant at a constant temperature and a section (in blue) through the phase tetrahedron at a constant oil-to-water ratio as a function of the main surfactant mass fraction γ_C and the co-surfactant mass fraction γ_D [28].

In the case of gelled microemulsions, the co-surfactant was added to the gelled sample at 25°C, which was then heated above the sol–gel transition temperature, where the sample was melted and could thus be mixed. After the gelation process (see Section *Sample Preparation*),

the phase behavior was recorded. While a gelled one-phase microemulsion appears transparent, the gelled two-phase samples are turbid.

In our experiments, the volume fraction of oil in the solvent mixture

$$\phi = \frac{V_{\mathrm{oil}}}{V_{\mathrm{water}} + V_{\mathrm{oil}}} \tag{1}$$

was kept constant at 0.50. The mass fraction of surfactant (C) is defined as

$$\gamma_{\mathrm{C}} = \frac{m_{\mathrm{surf.}}}{m_{\mathrm{water}} + m_{\mathrm{oil}} + m_{\mathrm{surf.total}} + m_{\mathrm{co-surf.}} + m_{\mathrm{gelator}}}, \tag{2}$$

where $m_{\mathrm{surf.}}$ is the active content of alkanoyl methylglucamides in the original surfactant formulation, while $m_{\mathrm{surf.total}}$ is the total mass of the technical-grade surfactant including co-solvents and additives. Then the mass fraction of the co-surfactant (D) is calculated by

$$\gamma_{\mathrm{D}} = \frac{m_{\mathrm{co-surf.}}}{m_{\mathrm{water}} + m_{\mathrm{oil}} + m_{\mathrm{surf.total}} + m_{\mathrm{co-surf.}} + m_{\mathrm{gelator}}}. \tag{3}$$

The salinity of the microemulsion sample is defined as

$$\varepsilon = \frac{m_{\mathrm{salt}}}{m_{\mathrm{water}} + m_{\mathrm{salt}}}. \tag{4}$$

The gelator mass fraction is calculated according to

$$\eta = \frac{m_{\text{gelator}}}{m_{\text{water}} + m_{\text{oil}} + m_{\text{surf.total}} + m_{\text{co-surf.}} + m_{\text{gelator}}}. \quad (5)$$

Small-angle neutron scattering (SANS)

The microstructure of selected microemulsions was investigated by small-angle neutron scattering (SANS). The microemulsion samples of $\gamma_C = 0.0521$, $\gamma_D = 0.0878$ with $\varepsilon = 0$ and $\gamma_C = 0.0689$, $\gamma_D = 0.0927$ with $\varepsilon = 0.0009$ were measured with the spectrometer NG7 at the National Institute of Standards and Technology (NIST), the USA. A neutron wavelength of $\lambda = 6$ Å with a wavelength spread of $\Delta\lambda/\lambda = 13.8\%$ (full width at half-maximum) was used. To cover a q-range from 0.002 to 0.48 Å, where $q = 4\pi \cdot \sin(\theta/2)/\lambda$ is the absolute value of the scattering vector, we chose the detector/collimation distances of 13.17 m/14.72 m, 4 m/8.52 m, and 1.33 m/5.42 m. The microemulsion samples of $\gamma_C = 0.0232$, $\gamma_D = 0.0737$ with $\varepsilon = 0$ and $\gamma_C = 0.0522$, $\gamma_D = 0.0878$ with $\varepsilon = 0.0009$ were measured with the instrument KWS-1 at the Heinz Maier-Leibniz Zentrum (MLZ) in Munich, Germany. Neutron wavelengths of $\lambda = 5$ and 10 Å with a wavelength spread of $\Delta\lambda/\lambda = 10\%$ were used to cover a q-range from 0.001 to 0.66 Å. The detector/collimation distances were 20 m/20 m, 8 m/20m and 1.5 m/8m. All samples were loaded into 1 mm Hellma quartz QS glass cells and then transferred to a cell holder with a high temperature precision and stability ($\Delta T = \pm 0.02$ K). It is ensured that samples have been in the homogeneous one-phase state during measurements by checking each sample before and after the measurement via visual inspection. The recorded scattering intensity was normalized to the absolute scale using the empty beam (for the data from NIST) and using the plexiglass (for the data from MLZ) as a reference. The raw data treatment, including the subtraction of the dark current and the empty cell scattering, masking, and radial averaging, was performed using the analysis software program IGOR Pro (for the data from NIST) and QtiSAS (for the data from MLZ). The detector dead time and sample transmission were also considered.

Rheology

Oscillatory shear rheometry was carried out with a rheometer Physica MCR 501 from Anton Paar, Austria. We used a plate-plate geometry, of which the upper plate has a diameter of 25 mm. The gap size between the two plates was kept constant at 1 mm according to previous experiments with gelled microemulsions [3]. Temperature can be controlled via an external thermostat with a precision of $\Delta T = \pm 0.1$ K. Firstly, an amplitude sweep was carried out at T = 25 °C with an angular frequency of $\omega = 10\ s^{-1}$ and a varied shear stress τ to determine the limit of the linear viscoelastic region (LVE region). For our gelled microemulsion samples, the limit of the LVE region is near $\tau = 40$ Pa. Hence, for subsequent measurements, the shear stress is kept constant at $\tau = 10$ Pa. Secondly, oscillation frequency sweeps were performed at T = 25 °C and $\tau = 10$ Pa as a function of the angular frequency ω. Lastly, a temperature sweep was carried out at an angular frequency of $\omega = 10\ s^{-1}$ and a shear stress of $\tau = 10$ Pa, from T = 25 °C to T = 100 °C with a heating rate of 1 K / min to determine the sol–gel transition temperature $T_{sol-gel}$, i.e. the temperature at which the values of G' and G'' decrease steeply.

Freeze-Fracture Electron Microscopy (FFEM)

In order to visualize the structure of the gelled non-toxic microemulsion with a transmission electron microscope, replicas of the specimen were prepared using the Freeze-Fracture and Etching System BAF060 from *Leica*. A small amount of the gelled microemulsion was placed on the two copper grids between two copper plates (4.5 mm × 3.0 mm) which were assembled to a so-called sandwich. Sandwiches were quickly frozen in liquid ethane. After fracturing in the liquid nitrogen, the grids with the frozen fractured specimen were fixed on a house-made specimen holder (with a metal cover plate to protect the specimens from contamination in the air) and quickly transferred into the vacuum chamber of the BAF060 (T = -150°C). The frozen fractured surface of the specimens was shadowed with platinum-carbon (~2 nm) at 45° and

covered by a layer of pure carbon (~20 nm) at 90°. The replicas were cleaned with warm ethanol, dried and examined with an EM10 transmission electron microscope from *Zeiss* operated at 60 kV.

Formulating non-toxic microemulsions with alkanoyl methylglucamides

Phase diagrams

The main task of this study was to formulate highly efficient non-toxic microemulsions using the relatively new class of alkanoyl methylglucamide surfactants. We chose three technical-grade surfactants, namely MEGA-8/10, MEGA-12/14-PC, and MEGA-12/14-HC, which differ in the hydrophobic chain length and the composition of the commercial products (see Section *Materials*). To study their ability to form microemulsions, we compare their phase diagrams with those of alkyl polyglucoside-containing microemulsions, which have been measured in our previous study [17]. The used technical-grade alkyl polyglucosides have the trademark Plantacare, namely Plantacare 810 UP ($C_{8/10}G_{1.5}$), Plantacare 2000 UP ($C_{10}G_{1.5}$), and Plantacare 1200 UP ($C_{12}G_{1.4}$). The influence of alkanoyl methylglucamides on the microemulsion phase behavior was first studied with the scouting system H_2O – *n*-octane – MEGA-8/10 –1-octanol and then with the non-toxic system H_2O – isopropyl myristate (IPM) – MEGA-12/14-PC – 1,2-octanediol and H_2O – IPM – MEGA-12/14-HC – 1,2-octanediol. As explained in Section *Phase Behavior*, the phase behavior of quaternary microemulsion systems at T = const. is represented in a phase tetrahedron (see Figure 2). We recall that the fishtail point $\tilde{X}$ $(\tilde{\gamma}_C, \tilde{\gamma}_D)$ is a measure of the system efficiency: the less surfactant and co-surfactant $(\tilde{\gamma}_C + \tilde{\gamma}_D)$ the system needs for the formation of the one-phase microemulsion, the higher its efficiency is. Since we intend to gel the one-phase bicontinuous microemulsion, the location of the fishtail point $\tilde{X}$ is of particular interest.

In the scouting system H_2O – *n*-octane – MEGA-8/10 – 1-octanol (see Figure 3, left), the co-surfactant mass fraction $\tilde{\gamma}_D$ at the point $\tilde{X}$ is 0.146, which is much higher than the value of 0.051 in the microemulsion H_2O – *n*-octane – Plantacare 810 UP ($C_{8/10}G_{1.5}$) – 1-octanol (see Figure 3, right). This means that MEGA-8/10 is substantially more hydrophilic than Plantacare 810 UP. The strong hydrophilicity of MEGA-8/10 is due to the fact that (a) one carbon of the hydrophobic chain of MEGA-8/10 belongs to the amide bond, i.e. the hydrophobic chain of MEGA-8/10 has one carbon less than Plantacare 810 UP, and (b) the head group is slightly more hydrophilic. However, the amount of the surfactant MEGA-8/10 ($\tilde{\gamma}_C = 0.045$) is smaller than that of Plantacare 810 UP ($\tilde{\gamma}_C = 0.070$). We suppose that the open-ring glucose head group of MEGA-8/10 allows for the formation of a denser surfactant film leading to a better shielding of the water/oil contact at the interface.

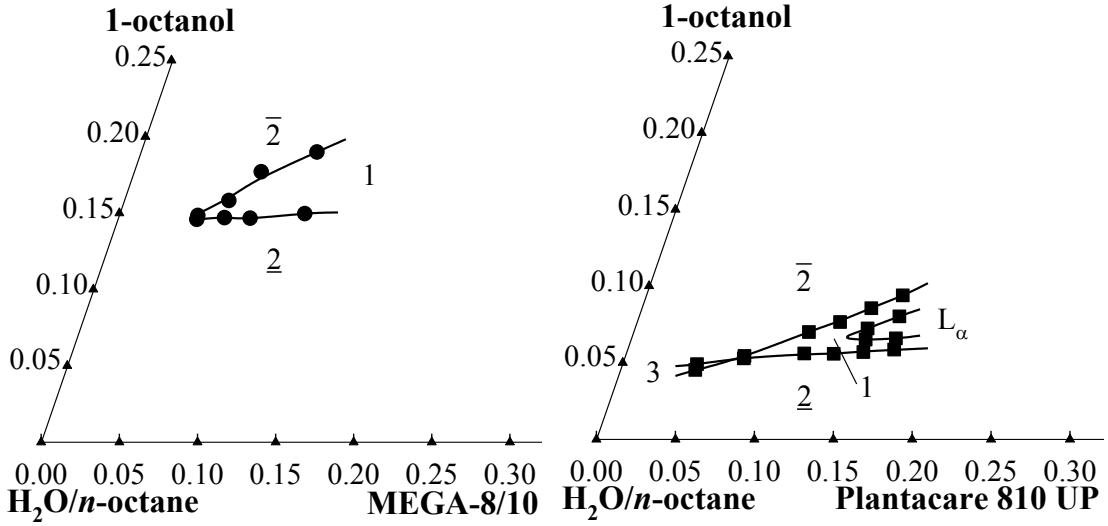

Figure 3. (left) Phase diagram of H_2O – *n*-octane – MEGA-8/10 – 1-octanol (circles) at T = 25°C, ϕ = 0.50. (right) Phase diagram of H_2O – *n*-octane – Plantacare 810 UP ($C_{8/10}G_{1.5}$) – 1-octanol (squares) at T = 25°C, ϕ = 0.50.

Having understood the influence of the glucamide surfactant on the microemulsion phase behavior in the scouting system, the next step was to study its influence on the non-toxic system. We have found the proper non-toxic components for the formation of sugar surfactant-containing microemulsions, namely IPM as the oil and 1,2-octanediol as the co-surfactant [17]. The oil IPM is more polar but has a longer alkyl chain than *n*-octane which results in a similar equivalent alkane chain number (EACN) [29]. Since furthermore the co-surfactant 1,2-octanediol is more hydrophilic than 1-octanol, MEGA-8/10 is expected to be less efficient in the non-toxic microemulsion than in the scouting system. In addition, the co-surfactant mass fraction $\tilde{\gamma}_D$ should further increase due to the larger monomeric solubility of 1,2-octanediol in IPM. Thus, we used MEGA-12/14-PC and MEGA-12/14-HC with a longer carbon chain length than MEGA-8/10 for the formulation of the non-toxic microemulsion (Figure 4, left). The phase diagrams of the non-toxic microemulsions H_2O – IPM – Plantacare – 1,2-octanediol are presented for comparison (Figure 4, right) [17]. As the hydrophobic chain of the Plantacare surfactant gets longer, the fish-tail points shift downwards to the left of the phase diagram, which indicates an efficiency increase of the system. Unlike the results of MEGA-8/10 and Plantacare 810 UP, MEGA-12/14-PC and Plantacare 1200 UP have similar efficiencies, with fishtail $\tilde{X}$ points of $(0.118, 0.094)$ and $(0.121, 0.098)$, respectively. This similarity is due to the shorter chain length of Plantacare which compensates (a) the C-atom that belongs to the head group and (b) the more hydrophilic head group of MEGA-12/14-PC as explained above (see also the CMC-curves in Figure S1 of the Supporting Information, which clearly indicate that the two surfactants have similar surface activities). On the other hand, MEGA-12/14-HC behaves completely different compared to MEGA-12/14-PC and Plantacare 1200 UP. The 3-phase region was not found in the microemulsion H_2O–IPM–MEGA-12/14-HC–1,2-octanediol, and the 1-phase microemulsion expands down to at least $\gamma_C = 0.0187$, $\gamma_D = 0.0611$. Thus, compared to the MEGA-12/14-PC containing microemulsion ($\tilde{\gamma}_C + \tilde{\gamma}_D \approx 0.21$), the

efficiency of the MEGA-12/14-HC containing microemulsion is surprisingly high ($\tilde{\gamma}_C + \tilde{\gamma}_D \leq 0.08$) although both products have the same main active component (see Section *Materials*). Note that the MEGA-12/14-HC containing samples were opaque at $\gamma_C \approx 0.019$ due to the strong scattering of the bicontinuous microemulsion.

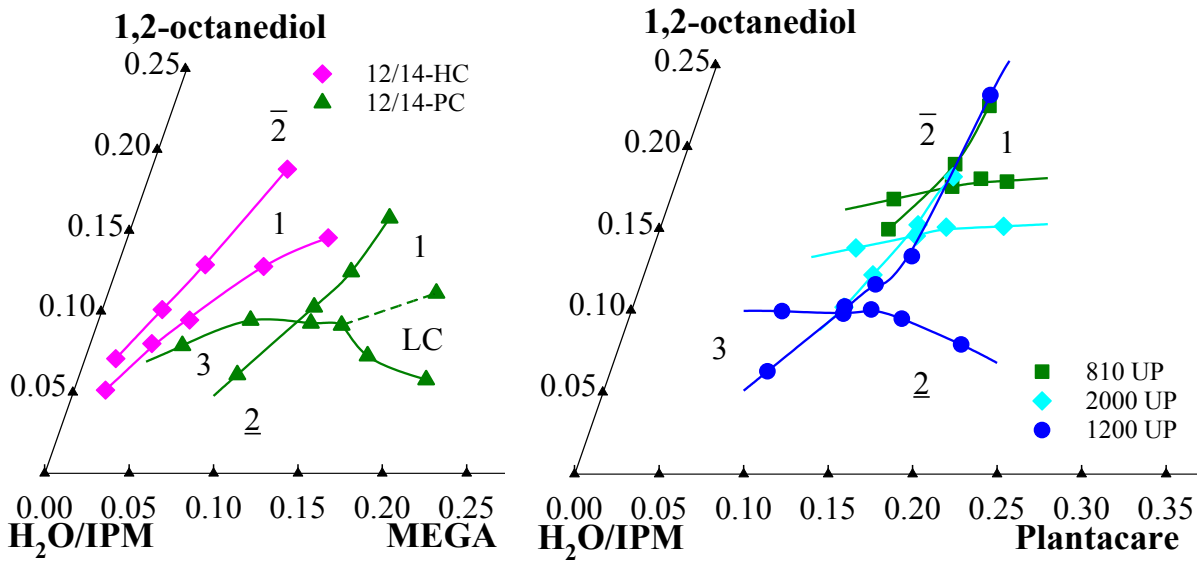

Figure 4. (left) Phase diagrams of H_2O – IPM – MEGA-12/14-PC – 1,2-octanediol (green triangles) and H_2O – IPM – MEGA-12/14-HC – 1,2-octanediol (pink diamonds) at T = 25°C, ϕ = 0.50. (right) Phase diagrams of H_2O – IPM – Plantacare 810 UP ($C_{8/10}G_{1.5}$) – 1,2-octanediol (green squares), H_2O – IPM – Plantacare 2000 UP ($C_{10}G_{1.5}$) – 1,2-octanediol (cyan diamonds), and H_2O – IPM – Plantacare 1200 UP ($C_{12}G_{1.4}$) – 1,2-octanediol (blue circles) at T = 25°C, ϕ = 0.50 [17].

An enormous efficiency improvement and the disappearance of the 3-phase region was also observed by Kaler et al. [30]. The surfactant efficiency increased by the factor of 4 in the microemulsion H_2O – *n*-decane – C_8E_3/didodecyl dimethylammonium bromide (DDAB) with 2% non-ionic surfactant C_8E_3 in the microemulsion H_2O – *n*-decane – C_8E_3 being replaced by

the cationic surfactant DDAB. However, adding a small amount of salt NaBr to the microemulsion H_2O – *n*-decane – C_8E_3/DDAB, the efficiency decreased to almost the same as that of the non-ionic microemulsion. Generally, the effect of these low salinities on the phase behavior is negligible; thus Kaler et al. inferred that the charge of DDAB modified the bending rigidity of the C_8E_3 monolayer (increase of efficiency) and that the addition of NaBr counterbalanced this effect (decrease of efficiency). Inspired by the work of Kaler, we suppose that the technical-grade surfactant contains traces of an ionic component which leads to a similar effect in the microemulsion H_2O – IPM – MEGA-12/14-HC – 1,2-octanediol, i.e. which increases the efficiency compared to the microemulsion H_2O – IPM – MEGA-12/14-PC – 1,2-octanediol. If this was the case, the addition of small amounts of salt would lead to a decrease in the efficiency.

In order to verify this assumption, microemulsions with salinities of $\varepsilon = 0.001, 0.002, 0.005$ were prepared. For the sake of clarity, only phase diagrams of H_2O – IPM – MEGA-12/14-HC – 1,2-octanediol and H_2O/NaCl – IPM – MEGA-12/14-HC – 1,2-octanediol with $\varepsilon = 0.001$ are presented in Figure 5, left. The phase boundaries of H_2O/NaCl – IPM – MEGA-12/14-HC – 1,2-octanediol with $\varepsilon = 0.002$ and $\varepsilon = 0.005$ have a similar shape to those with $\varepsilon = 0.001$ but shift to the right upper part of the phase diagram (see Figure S2 in SI). Fishtail $\tilde{X}$ points of all systems are summarized in Table 1. After adding salt, the 3-phase region appeared, which means the salt indeed counterbalanced the charge effects in the microemulsion. Moreover, the efficiency of the system decreases as the salinity increases but seems to level off approaching the $\tilde{\gamma}_C$ value of the MEGA-12/14-PC (see Table 1). For a clear view of the efficiency decrease tendency, $\tilde{\gamma}_C$ values at different salinities are plotted against the molar ratio of NaCl over MEGA-12/14-HC (Figure 5, right). These results support our assumption that the exceptional efficiency of MEGA-12/14-HC is caused by an unknown but tiny amount of an ionic amphiphilic component present in the surfactant formulation.

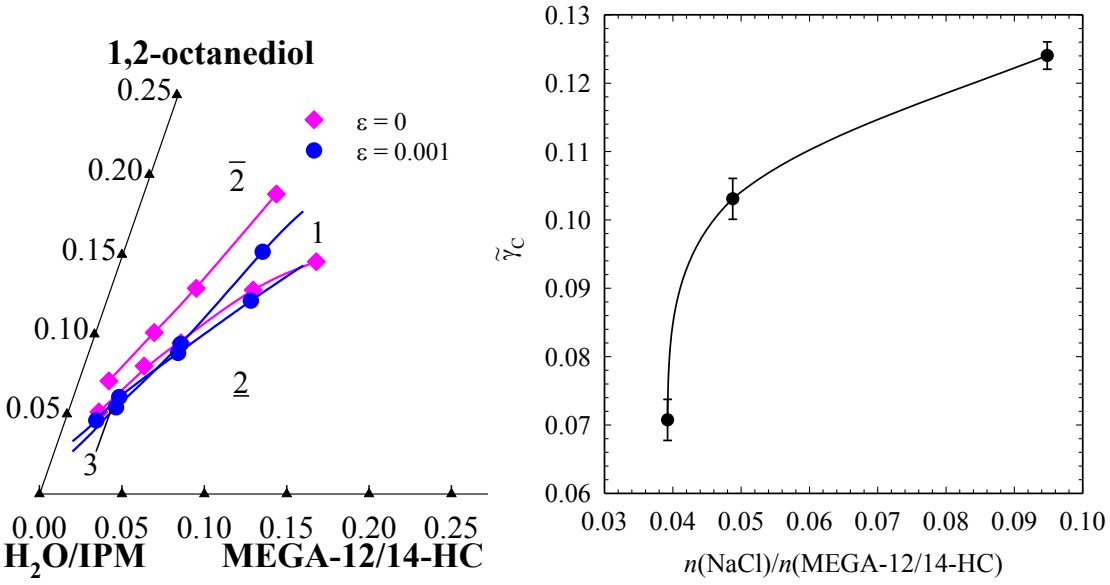

Figure 5. (left) Phase diagrams of H_2O – IPM – MEGA-12/14-HC – 1,2-octanediol (pink diamonds) and H_2O/NaCl – IPM – MEGA-12/14-HC – 1,2-octanediol with ε = 0.001 (blue circles) at T = 25°C, ϕ = 0.50. (right) Plot of $\tilde{\gamma}_C$ values against the molar ratio of NaCl over MEGA-12/14-HC for the microemulsion H_2O/NaCl – IPM – MEGA-12/14-HC – 1,2-octanediol.

Table 1. Summary of the fishtail $\tilde{X}$ points (the intersection point of the 3-phase and the 1-phase microemulsions) of all studied systems. Note that the volume fraction of oil in the water/oil mixture was adjusted to ϕ = 0.50.

Components				$\tilde{X}$ point	
H_2O	oil	surfactant	co-surfactant	$\tilde{\gamma}_C$	$\tilde{\gamma}_D$
	n-octane	MEGA-8/10	1-octanol	0.045	0.146
	n-octane	Plantacare 810 UP ($C_{8/10}G_{1.5}$)	1-octanol	0.070	0.051

	isopropyl myristate	MEGA-12/14-PC	1,2-octanediol	0.118	0.094
	isopropyl myristate	MEGA-12/14-HC	1,2-octanediol	-	-
	isopropyl myristate	Plantacare 810 UP ($C_{8/10}G_{1.5}$)	1,2-octanediol	0.152	0.173
	isopropyl myristate	Plantacare 2000 UP ($C_{10}G_{1.5}$)	1,2-octanediol	0.147	0.144
	isopropyl myristate	Plantacare 1200 UP ($C_{12}G_{1.4}$)	1,2-octanediol	0.121	0.098
NaCl in H_2O ($\varepsilon = 0.001$)	isopropyl myristate	MEGA-12/14-HC	1,2-octanediol	0.045	0.078
NaCl in H_2O ($\varepsilon = 0.002$)	isopropyl myristate	MEGA-12/14-HC	1,2-octanediol	0.069	0.103
NaCl in H_2O ($\varepsilon = 0.005$)	isopropyl myristate	MEGA-12/14-HC	1,2-octanediol	0.085	0.116

Microstructure determined via SANS

Since the system H_2O – IPM – MEGA-12/14-HC – 1,2-octanediol does not have a 3-phase region, it is hard to say whether a bicontinuous microstructure exists in the 1-phase microemulsion. Therefore, we carried out small-angle neutron scattering (SANS) experiments to investigate the microstructure as well as to observe the structural change induced by the composition change. For SANS measurements, H_2O must be replaced with D_2O to adjust bulk contrast. Generally, phase diagrams presented in volume fractions are supposed to remain almost the same in the deuterated system as in the protonated system. Hence, the salinity of $\varepsilon = 0.001$ in the protonated system was adjusted to $\varepsilon = 0.0009$ in the deuterated system. We checked the phase boundaries of the deuterated system to ensure the measured sample exhibits indeed a similar phase behavior (see Figure S3 in SI). Four samples with low γ located in the 1-phase region were measured: two for the microemulsion D_2O – IPM – MEGA-12/14-HC –

1,2-octanediol ($\gamma_C = 0.0521$, $\gamma_D = 0.0878$, $\phi = 0.50$ and $\gamma_C = 0.0232$, $\gamma_D = 0.0737$, $\phi = 0.50$) and two for the microemulsion D_2O/NaCl – IPM – MEGA-12/14-HC – 1,2-octanediol with $\varepsilon = 0.0009$ ($\gamma_C = 0.0689$, $\gamma_D = 0.0927$, $\phi = 0.50$ and $\gamma_C = 0.0522$, $\gamma_D = 0.0878$, $\phi = 0.50$). Figure 6 shows the scattering intensity plotted as a function of the scattering vector q in a double logarithmic representation. All four scattering curves have the typical shape known for bicontinuous microemulsions [6,31,32]: starting from low q-values, where the curves show a plateau, a scattering peak is found in the middle q-range before the intensity decreases proportional to q^{-4}, before the incoherent background is reached. The scattering peaks were analysed with the Teubner-Strey model (see SI) [31], yielding the periodicity of the oil and water domains d_{TS}, the correlations length ξ_{TS} and the amphiphilicity factor f_a.

The obtained fitting parameters are summarised in Table 2 together with the composition of the samples. Considering at first the scattering curves recorded for the two samples without salt (Figure 6, left), a strong shift of the correlation peak to larger q values is observed when the surfactant mass fraction is increased from $\gamma_C = 0.0232$ (empty circles) to $\gamma_C = 0.0521$ (empty squares). This result is expected as the distance between surfactant layers becomes smaller with increasing surfactant concentration. Accordingly, the periodicity d_{TS} decreases from 48.5 nm to 22.7 nm. Furthermore, the scattering peak of the sample at $\gamma_C = 0.0521$ is much more pronounced. This indicates that the microstructure is more ordered due to a weaker influence of thermal fluctuations which softens the amphiphilic film [33], and thus leads to a more negative amphiphilicity factor f_a. Note that the strong scattering of the very efficient microemulsion ($\gamma_C = 0.0232$) leads to double and multiple scattering contributions visible especially at $q \approx 2\, q_{max}$.

A similar trend is observed for the scattering curves of the two microemulsions with salt (Figure 6, right), i.e. the correlation peak shifts to larger q values when the surfactant mass

fraction increased from γ_C = 0.0522 (empty circles) to γ_C = 0.0689 (empty squares). Accordingly, both the periodicity and the correlation length decrease. However, due to the smaller difference in surfactant mass fraction the shift as well as the difference in d_{TS} and ξ_{TS} are much smaller. Last but not least, comparing the scattering curves of the samples with almost the same surfactant mass fraction but without and with salt (γ_C = 0.0521, γ_D = 0.0878, ε = 0 and γ_C = 0.0522, γ_D = 0.0878, ε = 0.0009), respectively, one finds similar values for the periodicity, the correlation length and the amphiphilicity. In summary, the recorded scattering curves indicate that even at very low surfactant mass fractions of γ_C = 0.0232 and γ_D = 0.0737 the microemulsion has a bicontinuous microstructure. The large length scale of the structure might be due to an increased bending rigidity of the amphiphilic film. We speculate that this increase is caused by an electrostatic repulsion, which, in turn, is induced by a tiny amount of an ionic amphiphilic component present in the surfactant formulation [30].

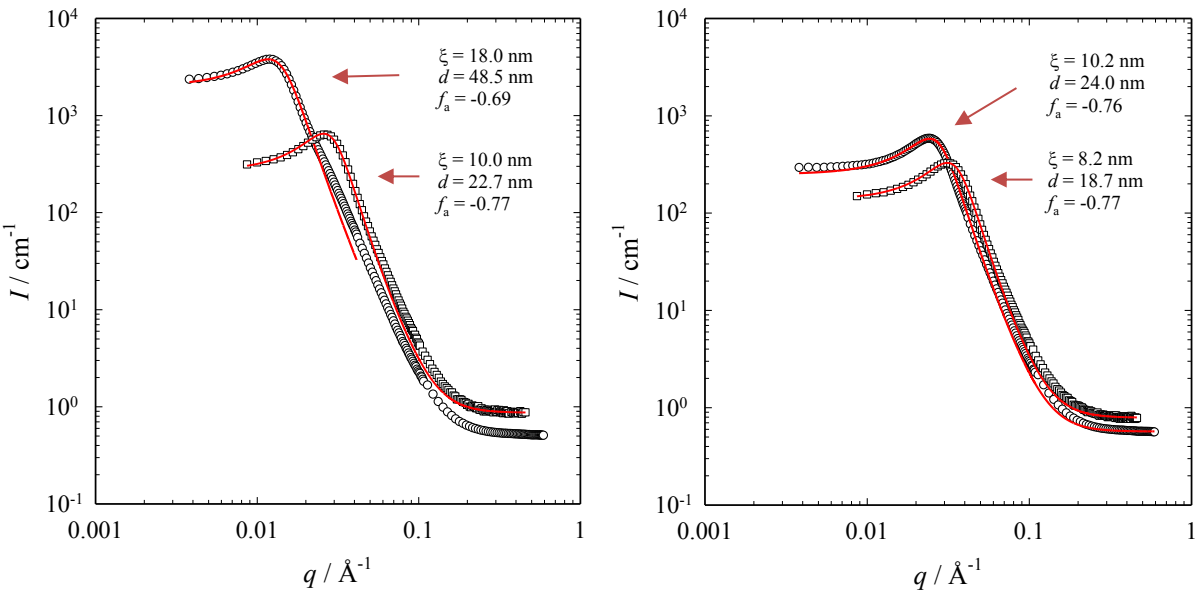

Figure 6. SANS curves of (left) D_2O – IPM – MEGA-12/14-HC – 1,2-octanediol with γ_C = 0.0232, γ_D = 0.0737, ϕ = 0.50 at T = 24.7 °C (empty circles) and γ_C = 0.0521, γ_D = 0.0878, ϕ = 0.50 at T = 27.0 °C (empty squares); (right) D_2O/NaCl – IPM – MEGA-12/14-HC – 1,2-

octanediol with $\gamma_C = 0.0522$, $\gamma_D = 0.0878$, $\varepsilon = 0.0009$, $\phi = 0.50$ at $T = 25.4$ °C (empty circles) and $\gamma_C = 0.0689$, $\gamma_D = 0.0927$, $\varepsilon = 0.0009$, $\phi = 0.50$ at $T = 27.0$ °C (empty squares). Red solid lines are Teubner-Strey fits [31].

Table 2. Composition of the samples (volume fraction of oil in solvent mixture ϕ, mass fraction of main surfactant γ_C, mass fraction of co-surfactant γ_D) as well as the correlation length ξ_{TS}, the periodicity d_{TS}, and the amphiphilicity factor f_a obtained from Teubner-Strey fits of the SANS data.

sample	ϕ	γ_C	γ_D	ξ_{TS} / nm	d_{TS} / nm	f_a
D_2O – IPM – MEGA-12/14-HC – 1,2-octanediol	0.5017	0.0521	0.0878	10.0	22.7	-0.77
	0.5000	0.0232	0.0737	18.0	48.5	-0.69
D_2O/NaCl – IPM – MEGA-12/14-HC – 1,2-octanediol ($\varepsilon = 0.0009$)	0.4992	0.0689	0.0927	8.2	18.7	-0.77
	0.5000	0.0522	0.0878	10.2	24.0	-0.76

Gelling non-toxic microemulsions

Having formulated the highly efficient non-toxic bicontinuous microemulsion H_2O – IPM – MEGA-12/14-HC – 1,2-octanediol, we intended to gel this microemulsion with a low molecular weight gelator and to examine its rheological properties. Finally, freeze-fracture electron microscopy (FFEM) was carried out to provide a direct image of the microstructure of the gelled microemulsion.

So far, there are no guiding rules on which low molecular weight gelators gels a specific solvent, i.e. finding a suitable gelator is still trial and error [5,34]. Since our microemulsion contains equal volumes of water and oil, theoretically both hydrogelator and organogelator could be suitable. In our previous study, the hydrogelator *N*, *N'*-dibenzoyl-L-cystine (DBC) did not gel

the non-toxic microemulsion H_2O – IPM – Plantacare 1200 UP – 1,2-octanediol at 2 wt.% but shifted the phase boundaries to a larger amount of co-surfactant. On the other hand, the organogelator 1,3:2,4-dibenzylidene-D-sorbitol (DBS) gelled the non-toxic microemulsion at 0.3 wt.% and the phase boundaries remained unchanged [17]. In the non-toxic microemulsion studied here (H_2O – IPM – MEGA-12/14-PC – 1,2-octanediol), the hydrogelator DBC also did not gel the system even at a gelator concentration as high as 3.0 wt.% but shifted the phase boundaries to a larger amount of co-surfactant (see Figure S4 in SI), which is consistent with the results for the glucoside-containing microemulsion. On the other hand, DBS gelled the non-toxic microemulsion H_2O – IPM – MEGA-12/14-HC – 1,2-octanediol and the phase boundaries remain unchanged (Figure 7), which is also consistent with the results for the glucoside-containing microemulsion. The gelled microemulsion even form at very low surfactant concentration ($\gamma_C = 0.019$, $\gamma_D = 0.06$, the left bottom end on the phase diagram). As already mentioned in connection with Figure 4 (left), the sample was opaque due to the strong scattering of the bicontinuous microemulsion. Nevertheless, the gelled 1-phase microemulsion was distinguishable from a gelled 2-phase microemulsion.

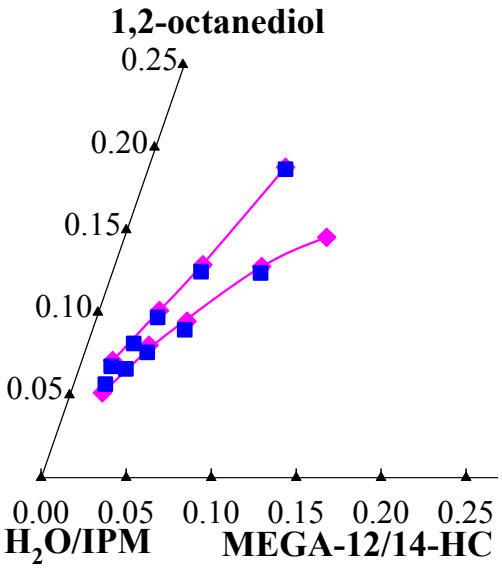

Figure 7. Phase diagrams of the non-gelled microemulsion H_2O–IPM–MEGA-12/14-HC–1,2-octanediol (pink diamonds) and the gelled microemulsion in the presence of DBS (blue squares) at $\eta = 0.003$, $T = 25°C$, $\phi = 0.50$.

After the formulation of the gelled non-toxic bicontinuous microemulsion, we performed oscillatory shear rheometry to examine the rheological properties. For this purpose, two compositions located in the middle of the 1-phase region were chosen, namely $\gamma_C = 0.0363$, $\gamma_D = 0.0885$ and $\gamma_C = 0.0538$, $\gamma_D = 0.1042$ in the presence of DBS at $\eta = 0.003$. The linear viscoelastic region (LVE) was determined in the preliminary amplitude sweep, and the shear stress was set at $\tau = 10$ Pa for the subsequent frequency sweep (Figure 8). The storage modulus *G'* is about one order of magnitude larger than the loss modulus *G''* over the entire frequency range and both moduli show only a very weak frequency dependence. The results show that the samples are i

ndeed gelled. Subsequently, a temperature sweep was carried out to characterize the sol-gel transition temperature $T_{sol-gel}$ (Figure 9). For both samples it is around 82 °C, where the storage modulus *G'* drops sharply and crosses the loss modulus *G''*. We thus conclude that the sol–gel transition temperature is $T_{sol-gel} \approx 82$ °C. The rheological properties of both samples do not differ significantly, which supports our assumption that our gelled non-toxic microemulsion is an orthogonal self-assembled system: (a) the gelator does not influence the phase behavior; (b) the bicontinuous microemulsion "only" acts as a solvent for the gelator, i.e. the rheological properties are determined by the gelator.

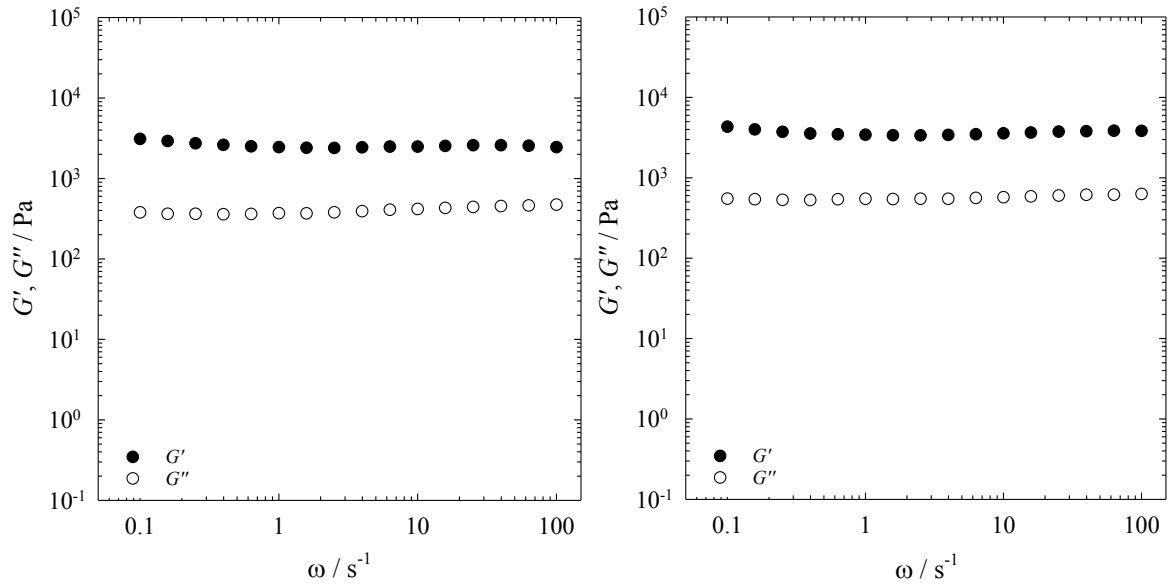

Figure 8. Storage modulus *G'* (filled symbols) and loss modulus *G''* (open symbols) of the gelled bicontinuous microemulsion H_2O – IPM – MEGA-12/14-HC – 1,2-octanediol in the presence of DBS at $\eta = 0.003$, $\tau = 10$ Pa, $T = 25$ °C as a function of ω with the composition of (left) $\gamma_C = 0.0363$, $\gamma_D = 0.0885$, $\phi = 0.50$; (right) $\gamma_C = 0.0538$, $\gamma_D = 0.1042$, $\phi = 0.50$.

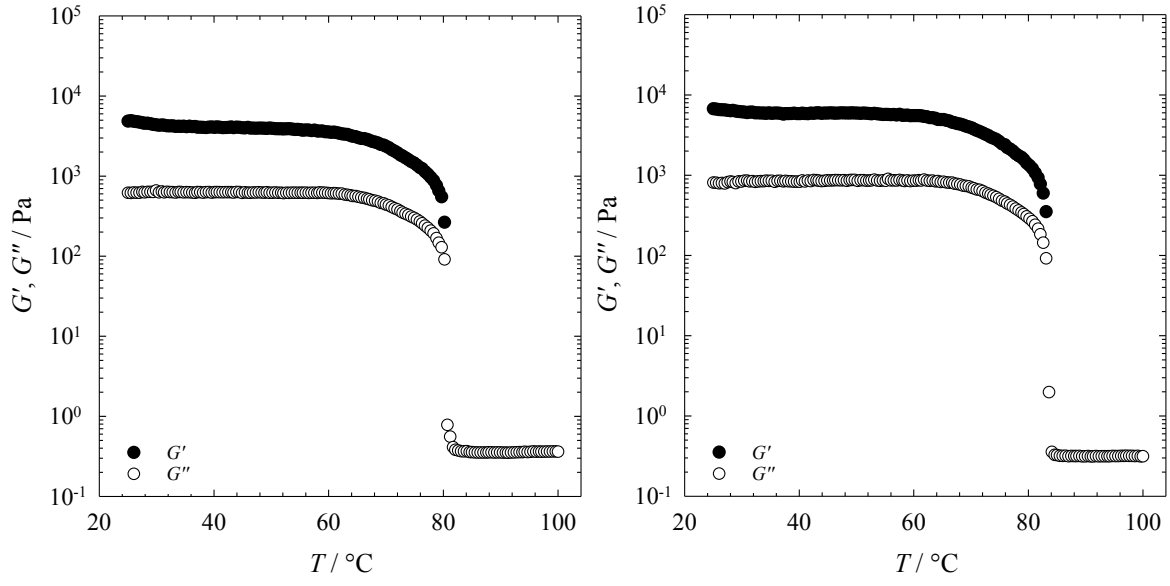

Figure 9. Storage modulus *G'* (filled symbols) and loss modulus *G''* (open symbols) of the gelled bicontinuous microemulsion H_2O – IPM – MEGA-12/14-HC – 1,2-octanediol in the

presence of DBS at $\eta = 0.003$, $\tau = 10$ Pa, $\omega = 10$ s^{-1} as a function of T and a heating rate of 1 °C min^{-1} with the composition of (left) $\gamma_C = 0.0363$, $\gamma_D = 0.0885$, $\phi = 0.50$; (right) $\gamma_C = 0.0538$, $\gamma_D = 0.1042$, $\phi = 0.50$.

To further study the microstructure of this new type of gelled non-toxic bicontinuous microemulsion, we used freeze-fracture electron microscopy (FFEM). The system of choice was H_2O – IPM – MEGA-12/14-HC – 1,2-octanediol ($\gamma_C = 0.0276$, $\gamma_D = 0.0774$, $\phi = 0.50$) in the presence of DBS at $\eta = 0.003$. Note that the surfactant mass fraction was chosen to be slightly larger than the one used in the SANS experiment to provide a wider one phase region for the FFEM sample preparation. The two representative FFEM picture shown in Figure 10 clearly prove the coexistence of both twisted gel fibers (red arrows) and bicontinuously structured regions (yellow circles). The gel fibers have diameters of $d_{fibril} \approx 8$–12 nm, which is consistent with the results obtained for the system H_2O – $C_{12}E_7$ in the presence of DBS at $\eta = 0.0075$ and $\eta = 0.015$ [35]. However, unlike the dense bundles of gel fibers in the system H_2O – $C_{12}E_7$ – DBS, the gel fibers in the system at hand are sparsely distributed (Figure 10, left) due to the very low gelator concentration ($\eta = 0.003$). Moreover, the length scale of the bicontinuous structure agrees almost quantitatively with the diameter of the water and the oil domains, respectively, obtained from SANS ($d_{TS}/2 \approx 24$ nm for a very similar sample). A closer inspection of the FFEM picture on the right side of Figure 10 reveals the existence of lamellar structured regions with a smaller periodicity. This finding suggests a partial phase separation of the sample during the FFEM sample preparation.

To conclude, not only the rheological and SANS measurements but also the freeze-fracture electron microscopy (FFEM) pictures show that this new type of gelled non-toxic bicontinuous

microemulsion is an orthogonal self-assembled system, i.e. both the gel fibers and the microemulsion structure form simultaneously but independently.

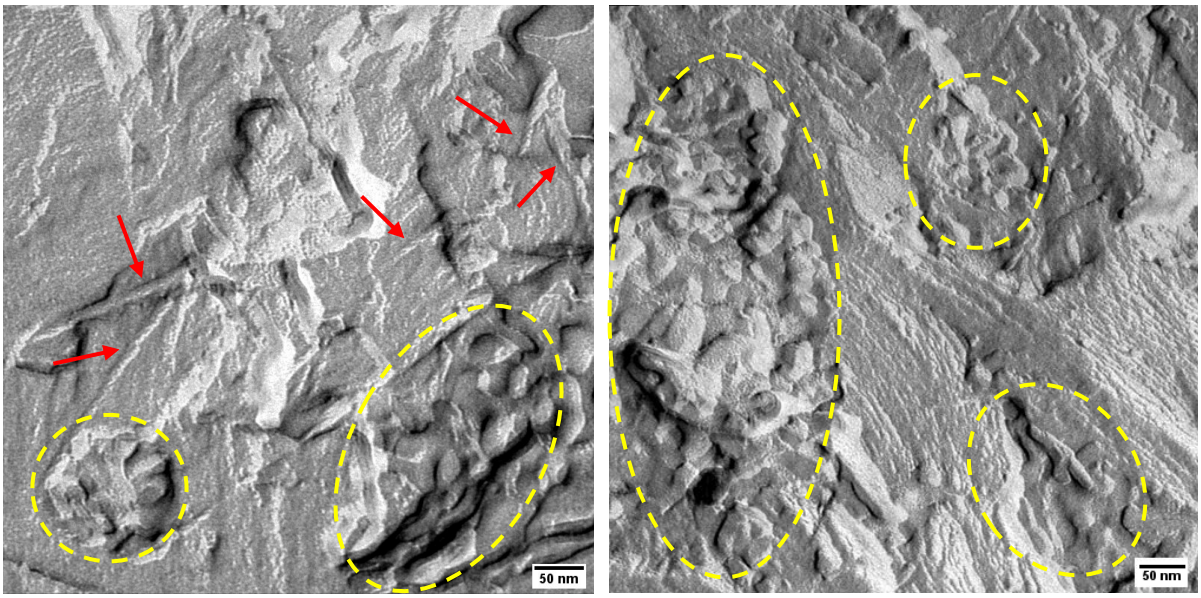

Figure 10. FFEM pictures of the gelled bicontinuous microemulsion H_2O – IPM – MEGA-12/14-HC – 1,2-octanediol in the presence of DBS at $\eta = 0.003$ with the composition of $\gamma_C = 0.0276$, $\gamma_D = 0.0774$, $\phi = 0.50$. The red arrows point at the gel fibers and the yellow circles show the bicontinuous microstructure.

Conclusion and Outlook

Gelled non-toxic bicontinuous microemulsions are interesting for transdermal drug delivery because the microemulsion facilitates the solubilization of both hydrophilic and hydrophobic drugs, while the gel network provides mechanical stability and an easy application. In our previous study, we formulated such a gelled system with H_2O – IPM – Plantacare 1200 UP ($C_{12}G_{1.4}$) – 1,2-octanediol in the presence of 0.3 wt.% DBS [17]. However, a large amount of Plantacare 1200 UP (12 wt.%) is needed to form a bicontinuous microemulsion. To overcome this drawback, we studied a relatively new class of surfactants, namely alkanoyl

methylglucamides. Unexpectedly, the efficiency increased largely while both the bicontinuous microstructure and the gel fibrillar network remained unchanged.

Since there are only very few studies about the phase behavior of alkanoyl methylglucamide (MEGA), we first compared MEGA-8/10 with the alkyl polyglucoside surfactant Plantacare 810 UP ($C_{8/10}G_{1.5}$) in the scouting system H_2O – *n*-octane – surfactant – 1-octanol. We found MEGA-8/10 to be substantially more hydrophilic than Plantacare 810 UP. Subsequently, we compared MEGA-12/14-PC and MEGA-12/14-HC (both have the same hydrophobic chain-length but differ in the formulations) with Plantacare 1200 UP ($C_{12}G_{1.4}$) in the non-toxic microemulsions H_2O – IPM – surfactant – 1,2-octanediol. Although the methylglucamide head group is more hydrophilic than the glucoside head group, MEGA-12/14-PC and Plantacare 1200 UP have similar efficiencies due to a slightly longer carbon chain-length of MEGA-12/14-PC. On the other hand, MEGA-12/14-HC has an exceptional efficiency of $\tilde{\gamma}_C + \tilde{\gamma}_D \leq 0.08$ but – surprisingly – does not form a 3-phase region. The 3-phase region appears after adding a small amount of salt, which, in turn, decreases the efficiency of the system. We thus speculate that the exceptional efficiency of MEGA-12/14-HC is caused by an electrostatic repulsion, which is induced by a tiny amount of an ionic amphiphilic component in the surfactant formulation.

After formulating the highly efficient non-toxic bicontinuous microemulsion, its bicontinuous microstructure was confirmed by small-angle neutron scattering (SANS) and freeze-fracture electron microscopy (FFEM), from which a periodicity of $d \approx 48$ nm could be determined. Furthermore, the system H_2O – IPM – MEGA-12/14-HC – 1,2-octanediol was gelled by the low molecular weight organogelator 1,3:2,4-dibenzylidene-D-sorbitol (DBS) at 0.3 wt.%. The phase boundaries of the gelled bicontinuous microemulsion remain unchanged compared to the non-gelled counterpart. The gelled bicontinuous microemulsions displayed the typical rheological behavior of gels with a sol–gel transition temperature of $T_{sol-gel} \approx 82$ °C.

In conclusion, all experimental results suggest that the new type of efficient gelled non-toxic bicontinuous microemulsion is an orthogonal self-assembled system, i.e. the gel fibrillar network and the bicontinuous microstructure form simultaneously but independently: (a) the gelator does not influence the phase behavior of the microemulsion; (b) the rheological properties of the gelled microemulsion are determined by the gelator and are independent of the microemulsion composition; (c) the bicontinuous oil and water domains coexist with twisted gel fibers as seen in the FFEM pictures.

In future studies, we will solubilize both hydrophilic and hydrophobic drugs in gelled non-toxic bicontinuous microemulsions and carry out skin permeability tests. Furthermore, we will investigate the rheological behavior and structure of gelled non-toxic bicontinuous microemulsions at various water-to-oil ratios. The main open question is whether DBS can be used for both water-rich and oil-rich microemulsions. If not, a proper gelator needs to be searched for in the first place. The final goal is to know how to formulate efficient gelled non-toxic bicontinuous microemulsion whose water- and oil-content can be adjusted as required.

ASSOCIATED CONTENT

Supporting Information. CMC curves of alkanoyl methylglucamides; phase diagrams of H_2O – IPM – MEGA-12/14-PC – 1,2-octanediol at different salinities; the location of SANS and FFEM samples on the phase diagram; the Teubner-Strey Model for SANS fittings; gelling H_2O – IPM – MEGA-12/14-PC – 1,2-octanediol with N, N'-dibenzoyl-L-cystine (DBC)

AUTHOR INFORMATION

Corresponding Author

*Cosima Stubenrauch, Email: cosima.stubenrauch@ipc.uni-stuttgart.de, phone: +49-711-685 64470.

Author Contributions

The manuscript was written through contributions of all authors. All authors have given approval to the final version of the manuscript.

Notes

The authors declare no competing financial interest.

ACKNOWLEDGMENTS

We thank Dr. Natascha Schelero from Clariant GmbH for providing the alkanoyl methylglucamide surfactants. We also thank Shih-Yu Tseng, Karina Abitaev, Diana Zauser for their valuable help with the SANS measurements. Furthermore, we would like to acknowledge the National Institute of Standards and Technology (NIST) in the USA and the Heinz Maier-Leibniz Zentrum (MLZ) in Munich, Germany for providing the facilities for the SANS measurements and the valuable support of the local contacts Dr. Yun Liu (NIST) and Dr. Henrich Frielinghaus (MLZ).

ABBREVIATIONS

CMC, critical micelle concentration; DBC, *N*, *N*'-dibenzoyl-L-cystine; DBS, 1,3:2,4-dibenzylidene-D-sorbitol; FFEM, freeze-fracture electron microscopy; IPM, isopropyl myristate; MEGA, alkanoyl methylglucamide; SANS, small-angle neutron scattering

REFERENCES

(1) Stubenrauch, C.; Gießelmann, F. Gelled Complex Fluids: Combining Unique Structures

with Mechanical Stability. *Angew. Chemie - Int. Ed.* **2016**, *55* (10), 3268–3275. https://doi.org/10.1002/anie.201506603.

(2) Laibinis, P. E.; Hickman, J. J.; Wrighton, M. S.; Whitesides, G. M. Orthogonal Self-Assembled Monolayers: Alkanethiols on Gold and Alkane Carboxylic Acids on Alumina. *Science* **1989**, *245* (4920), 845–847.

(3) Laupheimer, M.; Jovic, K.; Antunes, F. E.; da Graça Martins Miguel, M.; Stubenrauch, C. Studying Orthogonal Self-Assembled Systems: Phase Behaviour and Rheology of Gelled Microemulsions. *Soft Matter* **2013**, *9* (13), 3661. https://doi.org/10.1039/c3sm27883b.

(4) Laupheimer, M.; Sottmann, T.; Schweins, R.; Stubenrauch, C. Studying Orthogonal Self-Assembled Systems: Microstructure of Gelled Bicontinuous Microemulsions. *Soft Matter* **2014**, *10* (43), 8744–8757. https://doi.org/10.1039/C4SM01639D.

(5) Weiss, R. G. The Past, Present, and Future of Molecular Gels. What Is the Status of the Field, and Where Is It Going? *J. Am. Chem. Soc.* **2014**, *136* (21), 7519–7530. https://doi.org/10.1021/ja503363v.

(6) Strey, R. Microemulsion Microstructure and Interfacial Curvature. *Colloid Polym. Sci.* **1994**, *272* (8), 1005–1019. https://doi.org/10.1007/BF00658900.

(7) Heuschkel, S.; Goebel, A.; Neubert, R. H. H. Microemulsions—Modern Colloidal Carrier for Dermal and Transdermal Drug Delivery. *J. Pharm. Sci.* **2008**, *97* (2), 603–631.

(8) Kreilgaard, M.; Pedersen, E. J.; Jaroszewski, J. W. NMR Characterisation and Transdermal Drug Delivery Potential of Microemulsion Systems. *J. Control. release*

2000, *69* (3), 421–433.

(9) Kreilgaard, M. Influence of Microemulsions on Cutaneous Drug Delivery. *Adv. Drug Deliv. Rev.* **2002**, *54* (Suppl. 1), 77–98. https://doi.org/10.1016/S0169-409X(02)00116-3.

(10) Kogan, A.; Garti, N. Microemulsions as Transdermal Drug Delivery Vehicles. *Adv. Colloid Interface Sci.* **2006**, *123*, 369–385.

(11) Callender, S. P.; Mathews, J. A.; Kobernyk, K.; Wettig, S. D. Microemulsion Utility in Pharmaceuticals: Implications for Multi-Drug Delivery. *Int. J. Pharm.* **2017**, *526* (1–2), 425–442. https://doi.org/10.1016/j.ijpharm.2017.05.005.

(12) Kahlweit, M.; Busse, G.; Faulhaber, B. Preparing Microemulsions with Lecithins. *Langmuir* **1995**, *11* (5), 1576–1583. https://doi.org/10.1021/la00005a027.

(13) Kahlweit, M.; Busse, G.; Faulhaber, B. Preparing Microemulsions with Alkyl Monoglucosides and the Role of N-Alkanols. *Langmuir* **1995**, *11* (9), 3382–3387. https://doi.org/10.1021/la00009a019.

(14) Kahlweit, M.; Busse, G.; Faulhaber, B.; Eibl, H. Preparing Nontoxic Microemulsions. *Langmuir* **1995**, *11* (11), 4185–4187.

(15) Kahlweit, M.; Busse, G.; Faulhaber, B. Preparing Nontoxic Microemulsions with Alkyl Monoglucosides and the Role of Alkanediols as Cosolvents. *Langmuir* **1996**, *12* (4), 861–862.

(16) Kahlweit, M.; Busse, G.; Faulhaber, B. Preparing Nontoxic Microemulsions. 2. *Langmuir* **1997**, *13* (20), 5249–5251. https://doi.org/10.1021/la970583z.

(17) Peng, K.; Sottmann, T.; Stubenrauch, C. Gelled Non-Toxic Microemulsions: Phase

Behavior & Rheology. *Soft Matter* **2019**, *15* (41), 8361–8371. https://doi.org/10.1039/c9sm01350d.

(18) Okesola, B. O.; Vieira, V. M. P.; Cornwell, D. J.; Whitelaw, N. K.; Smith, D. K. 1,3:2,4-Dibenzylidene- <scp>d</Scp> -Sorbitol (DBS) and Its Derivatives – Efficient, Versatile and Industrially-Relevant Low-Molecular-Weight Gelators with over 100 Years of History and a Bright Future. *Soft Matter* **2015**, *11* (24), 4768–4787. https://doi.org/10.1039/C5SM00845J.

(19) Sottmann, T.; Kluge, K.; Strey, R.; Reimer, J.; Söderman, O. General Patterns of the Phase Behavior of Mixtures of H2O, Alkanes, Alkyl Glucosides, and Cosurfactants. *Langmuir* **2002**, *18* (8), 3058–3067. https://doi.org/10.1021/la011665x.

(20) Reimer, J.; Söderman, O.; Sottmann, T.; Kluge, K.; Strey, R. Microstructure of Alkyl Glucoside Microemulsions: Control of Curvature by Interfacial Composition. *Langmuir* **2003**, *19* (26), 10692–10702. https://doi.org/10.1021/la034847v.

(21) Jakobs, B.; Sottmann, T.; Strey, R.; Allgaier, J.; Willner, L.; Richter, D. Amphiphilic Block Copolymers as Efficiency Boosters for Microemulsions. *Langmuir* **1999**, *15* (20), 6707–6711. https://doi.org/10.1021/la9900876.

(22) Sottmann, T. Solubilization Efficiency Boosting by Amphiphilic Block Co-Polymers in Microemulsions. *Curr. Opin. Colloid Interface Sci.* **2002**, *7* (1–2), 57–65. https://doi.org/10.1016/S1359-0294(02)00003-1.

(23) Söderman, O.; Johansson, I. Polyhydroxyl-Based Surfactants and Their Physico-Chemical Properties and Applications. *Curr. Opin. Colloid Interface Sci.* **1999**, *4* (6), 391–401. https://doi.org/10.1016/S1359-0294(00)00019-4.

(24) Hill, K.; Rhode, O. Sugar-Based Surfactants for Consumer Products and Technical Applications. *Fett-Lipid* **1999**, *101* (1), 25–33. https://doi.org/10.1002/(SICI)1521-4133(19991)101:1<25::AID-LIPI25>3.3.CO;2-E.

(25) Yang, X. D.; Gao, Y. H.; Chai, J. L.; Wang, Z. N.; Qin, C. K. Studies on the Middle-Phase Microemulsion of Lauric-N-Methylglucamide. *Colloid J.* **2007**, *69* (2), 252–258. https://doi.org/10.1134/S1061933X07020172.

(26) Yang, X.; Li, H.; Chai, J.; Gao, Y.; Chen, J.; Lou, A. Phase Behavior Studies of Quaternary Systems Containing N-Lauroyl-N-Methylglucamide/Alcohol/Alkane/Water. *J. Colloid Interface Sci.* **2008**, *320* (1), 283–289. https://doi.org/10.1016/j.jcis.2007.12.043.

(27) Yang, X.; Zhang, H.; Shi, C.; Chai, J. Middle-Phase Microemulsions Formed by n-Dodecyl Polyglucoside and Lauric-N-Methylglucamide. *J. Dispers. Sci. Technol.* **2013**, *34* (2), 147–152. https://doi.org/10.1080/01932691.2011.653927.

(28) Kluge, K.; Stubenrauch, C.; Sottmann, T.; Strey, R. Temperature-Insensitive Microemulsions Formulated from Octyl Monoglucoside and Alcohols : Potential Candidates for Practical Applications. *Tenside Surf. Det.* **2001**, *38* (1), 30–40.

(29) Aubry, J. M.; Ontiveros, J. F.; Salager, J. L.; Nardello-Rataj, V. Use of the Normalized Hydrophilic-Lipophilic-Deviation (HLDN) Equation for Determining the Equivalent Alkane Carbon Number (EACN) of Oils and the Preferred Alkane Carbon Number (PACN) of Nonionic Surfactants by the Fish-Tail Method (FTM). *Adv. Colloid Interface Sci.* **2020**, *276*. https://doi.org/10.1016/j.cis.2019.102099.

(30) Silas, J. A.; Kaler, E. W. The Phase Behavior and Microstructure of Efficient Cationic - Nonionic Microemulsions. *J. Colloid Interface Sci.* **2001**, *243* (1), 248–254.

https://doi.org/10.1006/jcis.2001.7874.

(31) Teubner, M.; Strey, R. Origin of the Scattering Peak in Microemulsions. *J. Chem. Phys.* **1987**, *87* (5), 3195–3200. https://doi.org/10.1063/1.453006.

(32) Sottmann, T.; Strey, R. Ultralow Interfacial Tensions in Water–n-Alkane–Surfactant Systems. *J. Chem. Phys.* **1997**, *106* (20), 8606–8615. https://doi.org/10.1063/1.473916.

(33) Morse, D. C. Topological Instabilities and Phase Behavior of Fluid Membranes. *Phys. Rev. E* **1994**, *50* (4), R2423.

(34) Draper, E. R.; Adams, D. J. Low-Molecular-Weight Gels: The State of the Art. *Chem* **2017**, *3* (3), 390–410. https://doi.org/10.1016/j.chempr.2017.07.012.

(35) Steck, K.; Preisig, N.; Stubenrauch, C. Gelling Lyotropic Liquid Crystals with the Organogelator 1,3:2,4-Dibenzylidene-d-Sorbitol Part II: Microstructure. *Langmuir* **2019**, *35* (52), 17142–17149. https://doi.org/10.1021/acs.langmuir.9b03346.

For Table of Contents Only